Chapter 1
Water-Specific Imaging

Keywords Nondestructive water image · Neutron beam image · Water-specific image · Root image in soil · 3D water image · 3D root image · Water in flower · Water in wood disk · Water absorption in seeds

1.1 Neutron Beam Imaging

When collimated neutrons are used to irradiate the sample, the neutrons penetrating the sample can produce images on film or transmit them to a computer through a CCD camera based on the intensity of the neutrons. The neutron beam image can be expressed as a kind of shade if it can be compared to shade images of light. To obtain a high-resolution neutron image, a parallel beam with high quality is needed, which is primarily decided by the features of the neutron collimator. When the length of the collimator is L and the aperture size of the collimator is D, the resolution of the image is reciprocal to L/D. To increase the resolution, it is preferable to use collimators with an L/D of more than 100. Another way to increase the resolution is to reduce the distance between the sample and the film or a camera. The resolution of the imaging time is dependent on the neutron flux and reciprocal to $(L/D)^2$. Another factor that can deteriorate the resolution is movement of the sample itself during the imaging. In the case of plant samples, the development of the tissue is not so fast; therefore, the imaging time is not as critical compared to the case of samples of engineering substances, such as imaging the formation of bubbles in the hot water in a metal pipe.

The features of a neutron beam compared to that of an X-ray are shown in Fig. 1.1, where the neutron attenuation coefficient, indicating the difficulty in penetrating the elements, is plotted in a log-scale manner. Generally, the penetration rate of metals is high for neutrons, and a small amount of neutrons could penetrate the light elements, which overall is roughly the reverse of that of an X-ray.

Supplementary Information The online version of this chapter (https://doi.org/10.1007/978-981-33-4992-6_1) contains supplementary material, which is available to authorized users.

T. M. Nakanishi, *Novel Plant Imaging and Analysis*,
https://doi.org/10.1007/978-981-33-4992-6_1

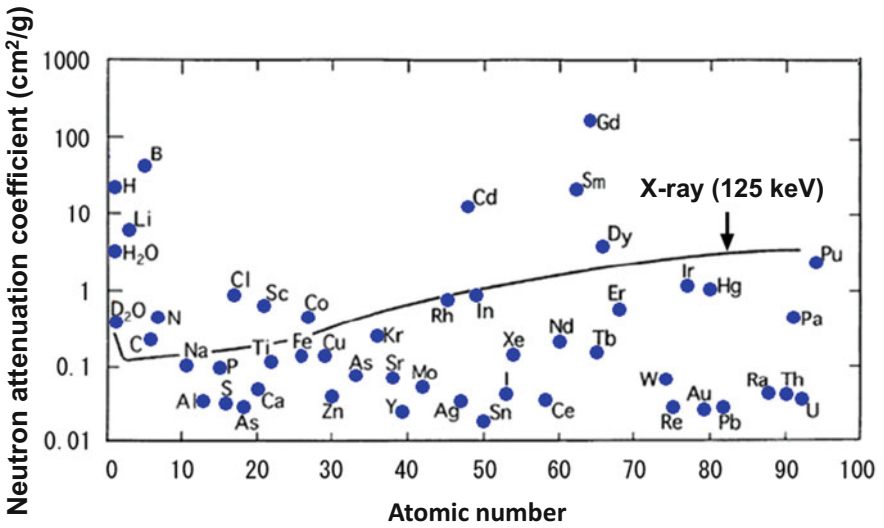

Fig. 1.1 Thermal neutron attenuation coefficient

As shown in Fig. 1.1, the attenuation coefficient of some light elements, including hydrogen, as well as rare earth elements, is extremely high, 100–1000 times higher than those of the other common elements. Because of the selective nuclear reaction of the neutron beam, when the neutron beam is used to irradiate the samples, including light elements or rare earth elements, the beam intensity is drastically reduced after penetrating the sample, which resulted in a clear image of these elements in the sample. In the case of X-rays, the beam reacts with electrons occupying the outside of the nuclide of the element. Since the number and density of the electrons increase with the atomic number of the element, the reaction of the X-ray with electrons increases, which results in a higher attenuation coefficient. Therefore, in the case of X-rays, this attenuation coefficient changes by factors, not by order of magnitudes, from lighter elements to heavier elements, which makes it difficult to distinguish the image of a specific element from that of the neighboring other elements.

Then, what can we see inside a plant irradiated with a neutron beam? In addition to hydrogen, there are only minimal amounts of lithium, boron or rare earths to attenuate neutron beams in plants. Therefore, the neutron beam can be regarded as producing a hydrogen image selectively. Since more than 80% of a living cell consists of water, the hydrogen image from plants is almost entirely water. After complete dehydration, there was hardly any neutron image in most of the plant samples. Therefore, we could regard the neutron image as a water-specific image. The acquired neutron image not only showed water distribution but also indicated the morphological development of the tissue itself. The following section shows how neutron beam images of intact plant tissues can give exquisite microscopic images never seen before.

1.2 Water-Specific Images by Neutron Beam

As written above, when a plant is irradiated with thermal neutrons, the neutron attenuation coefficient changes with the water content in the plant, producing different exposure images on an X-ray film. The different exposure images exhibit different levels of whiteness in an X-ray film; therefore, the whiteness of the film indicates changes in the water content in the tissue. This means that the water content can be estimated from the extent of whiteness in the image.

Figure 1.2 shows a schematic illustration of neutron radiography. When the sample was irradiated with a neutron beam, the neutrons penetrated after the sample produced an image on the X-ray film. The first trial used this kind of facility so that in the case of the plant sample, the sample had to be grown in a thin container to minimize the superposing water image around the roots.

The preparation of the sample and the irradiation method are described below with a soybean plant as an example. To obtain the neutron image of roots imbedded in soil, a soybean seedling was transplanted to a thin aluminum container (50 × 150 mm, 3 mm in thickness) packed with Toyoura's standard sand (silt type, 197–203 μm, in pore size) containing 15% (w/w) water. The upper part of the container was covered with aluminum tape to prevent water loss due to evaporation. The samples were kept at 26 °C under 70% humidity with 20,000 lux of light

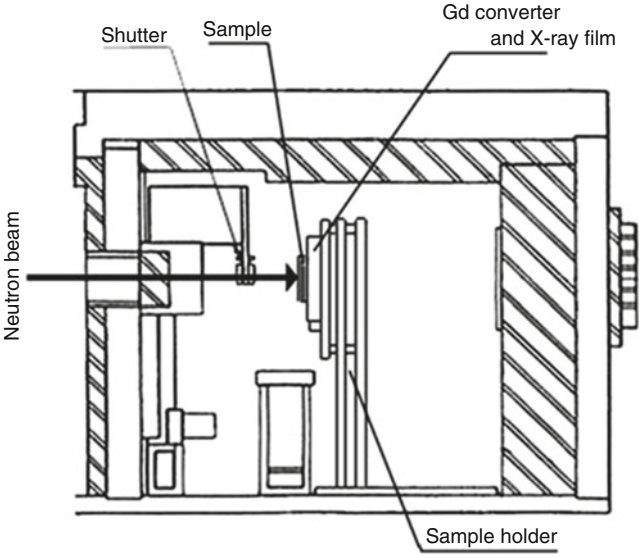

Fig. 1.2 Schematic illustration of the neutron irradiation chamber for neutron radiography [1]. The neutron beam from a reactor was irradiated from the left side to the sample, which was fixed on the cassette. After penetrating the sample, the neutrons were converted to radiation by a Gd n/γ converter set before an X-ray film in a cassette. Then, by developing the X-ray film, the image produced on the X-ray film was acquired

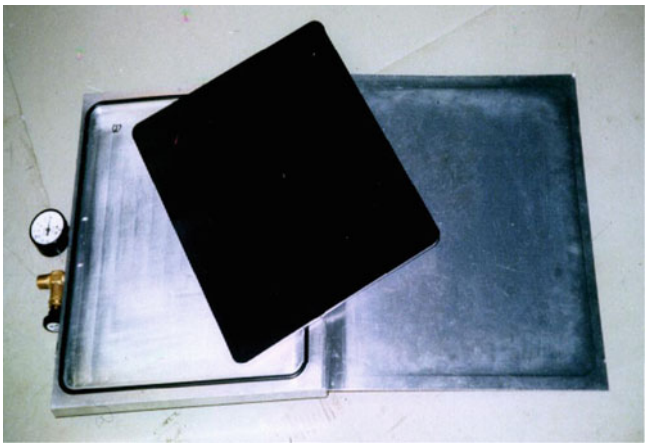

Fig. 1.3 Gadolinium converter and a cassette. The gadolinium (Gd) converter was prepared by depositing gadolinium on an aluminum plate (25 μm in thickness) and coated with sapphire to prevent oxidation. When irradiated with neutrons, gadolinium emits β-rays (conversion electrons) and γ-rays. The X-ray film is mainly exposed to β-rays to produce the image. The Cd converter and an X-ray film were placed in a cassette and sealed in vacuum

in a growth chamber. The plant sample was fixed to an aluminum cassette where a gadolinium n/γ converter and an X-ray film were sealed in vacuum (Figs. 1.3 and 1.4). The gadolinium converter was prepared by depositing gadolinium on an aluminum plate (25 μm in thickness) and was coated with sapphire to prevent oxidation. When irradiated with neutrons, gadolinium emits β-rays (conversion electrons) and gamma-rays, and the X-ray film is exposed mainly by the β-rays to produce the image. Therefore, the emulsion side of the film was placed tightly on the gadolinium side of the converter in the cassette.

The cassette was set vertically and was irradiated by thermal neutrons from an atomic reactor, JRR-3 M, installed at the Japan Atomic Energy Agency (JAEA) (Fig. 1.2). The total neutron flux was 1.9×10^8 n/cm^2.

After irradiation, the aluminum container became radioactive due to ^{28}Al formation, with a half-life of 2.3 m. However, after 15 m, the radioactivity of the sample was reduced to the background level. The plant samples themselves did not become radioactive after irradiation because the total irradiating neutron flux was relatively low. After irradiation, the film was developed, and the image was scanned by a scanner. When these irradiated plants were left to continue their growth, there was no observable effect compared with unirradiated plants.

1.2.1 2-Dimensional Images of Roots

When the growth of roots imbedded in soil could be visualized, we expected to determine new plant activities, since plant physiology has been developed mainly

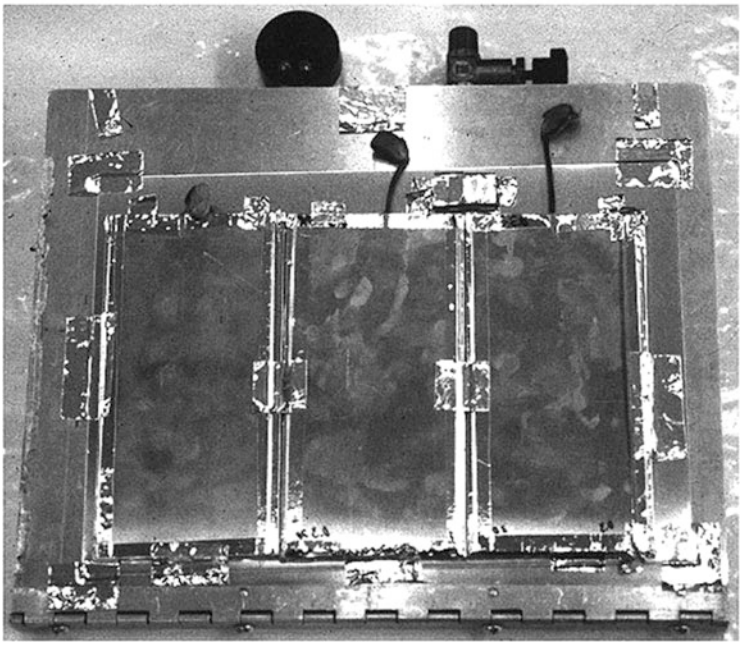

Fig. 1.4 Plant samples prepared for neutron radiography. Since the Al board does not produce figures by neutron irradiation, the samples were prepared on an Al board, and this board was fixed on the cassette by Al tape. In the case of a soybean plant, the samples were grown in a thin aluminum container (50 × 150 × 3 mm) where Toyoura's standard sand (silt type, 197–203 μm, in pore size) containing 15% (w/w) of water was packed. The sample was kept in a phytotron and periodically removed to perform neutron imaging

depending on water culture, where the nutritional conditions can be strictly defined. However, plants growing in the field are influenced by soil conditions, matrix features, nutrient conditions, water amount, etc. All of these conditions differ from place to place and depend on season or climate. However, the physiology of plants growing in the field is not well known, and some of the information is from an agricultural perspective, i.e., how to obtain high yield. Is there any relationship between the growth of the aboveground part and that of the root? Is there any preference regarding the physical condition of the soil for growth? There are many questions to be solved for the plants growing in soil from the perspective of plant physiology. The visualization of roots imbedded in soil could be visualized, provide clues to solve these questions. Therefore, we tried to visualize what we usually cannot see by utilizing neutrons. The following is an example of the root images in soil taken by a neutron beam.

Figure 1.5 shows a neutron image of a soybean plant in an aluminum container 3 mm in thickness. The whiteness in the figure corresponds to the water amount; therefore, the lighter part corresponds to regions where the water content is higher. Since the water content in the roots is much higher than that of the surrounding sand,

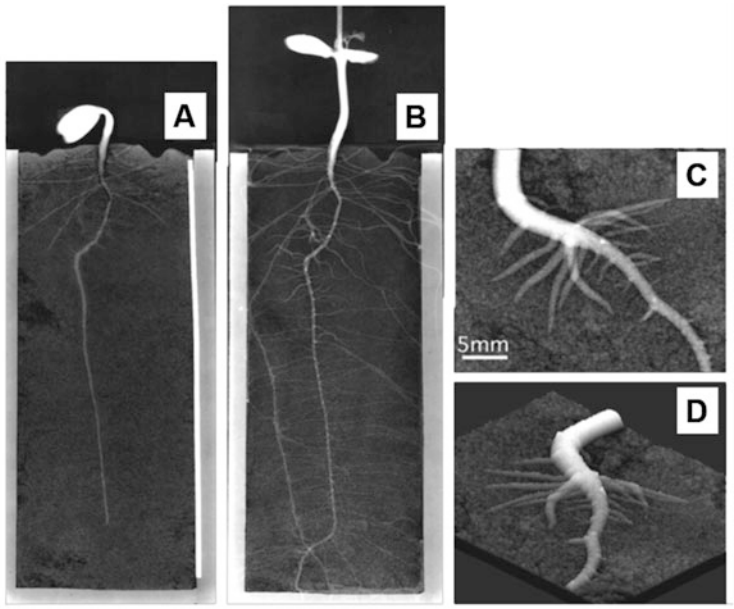

Fig. 1.5 Neutron images of soybean roots embedded in soil [2]. (**a** and **b**) the soybean plant images after 8 and 15 days. The whiteness in the figure corresponds to the water amount; therefore, the whiter part corresponds to the site with higher water content. Since the water concentration in the roots was higher than that in the soil, the morphological development of the roots and water movement were analyzed from the images. (**c**) magnification of the root when side roots emerged to develop. (**d**) conversion of the upper image to a 3-dimensional image, where the water amount was employed as the height

the root image is clearly shown in the figure even in the presence of soil. A water-deficient region, which was indicated as a darker site in the image, is clearly shown near the upper part of the main root.

The neutron image of the root imbedded in soil provides two pieces of information: the morphological development of the root and the water profile in the soil. As shown in the figure, we could visualize how the roots developed after the 8th day and 15th day of germination. The white dots shown in the main root indicate that a side root grew from this site and was superposed on the main root.

To discern the water content of the root more clearly, a part of the magnified root of the soybean plant 8 days after germination is shown. The three-dimensional image was acquired by processing the 2D figure of the root, and the height of the image corresponds to the whiteness and the amount of water. The 3D image showed more clearly that the water in the vicinity of the root, where the secondary root was developing, was taken up actively by the root, as shown by the clear emergence of the secondary root.

Figure 1.6 shows the morphological variety of soybean root images. Usually, balanced development of the lateral roots between both sides of the main root is

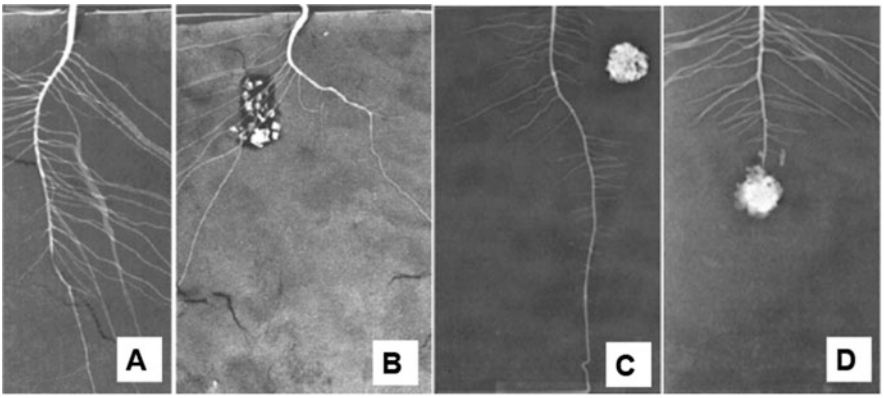

Fig. 1.6 Morphological differences of soybean roots embedded in soil. The balanced development of the lateral roots between both sides of the main root is commonly shown. However, when there is any change in soil condition on one side of the main root, the development of this side of the lateral roots changes from that of the other side. When there is some change near the root tip, the main root development ceases, but the lateral roots develop well to compensate for the ceased development of the main root. (**a**) control sample; (**b**) water-absorbing polymer containing water was placed on one side of the main root; (**c**, **d**) water-absorbing polymer containing 50 mM vanadium solution was placed on one side of the main root and in front of the root tip

shown. However, when there is any change in the soil condition in the vicinity of the main root, the development of one side of the lateral roots differs from that of the other side. For example, with enough water near the main root supplied from the water-absorbing polymer, the lateral roots on this side developed so well that some of them were even penetrating the water-absorbing polymer. On the other hand, when a heavy metal solution (water-absorbing polymer containing 50 mM vanadium) was placed on one side of the main root, the development of the lateral roots on this side ceased (Fig. 1.6c). In other cases, when this kind of polymer containing vanadium was placed just in front of the main root tip, the main root development stopped, but the lateral roots developed well, as if to compensate for the halted development of the main root (Fig. 1.6d).

These nondestructive images of root development in soil were applied to evaluate the effect of soil conditioning agents or water absorption polymers from the morphological development pattern of the roots or the change in water amount in soil. An earlier example is the effect of new lignin derivatives as soil conditioning agents in an acidic soil where aluminum ions inhibit plant growth1). Dissolved Al in soil is one of the major factors limiting crop production in acidic soil, which represents approximately 30–40% of the soil usable for agriculture in the world. To evaluate the effect of the soil conditioning agent under acidic soil conditions, the radish (*Raphanus sativus* var. *radicula* Pers.) was grown in soil containing lignin modified by radical sulfonation and alkaline oxygen treatment. Then, the root image obtained by the neutron beam was acquired. Figure 1.7 shows the traced images of the root acquired by neutron irradiation, and from these images, the root length was obtained

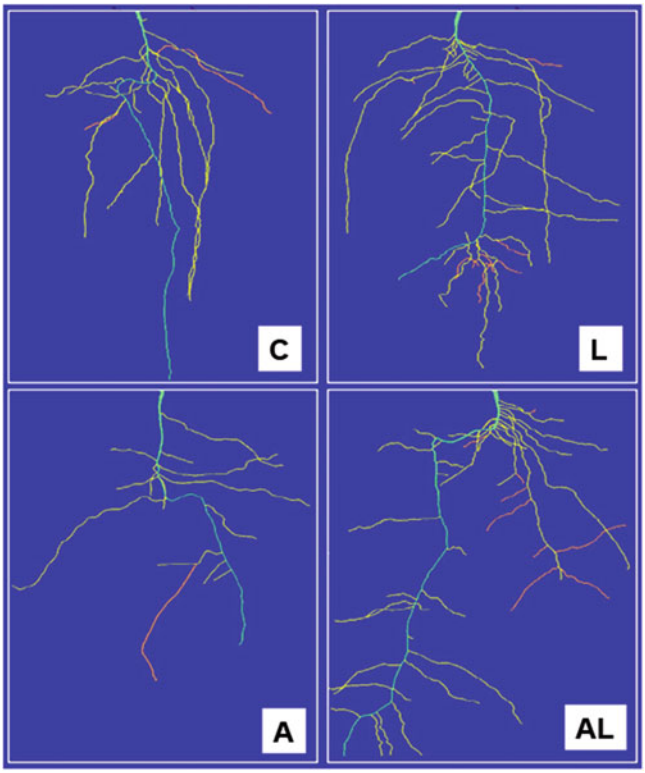

Fig. 1.7 Traced image of the radish roots acquired in neutron images [3]. The main root was colored blue, and the second and third roots were colored yellow and red. The effect of soil conditioning agents was observed from the morphological development pattern of the roots or the change in water amount in the soil. *C* control sample, *L* lignin derivatives (prepared as soil conditioning agents) were supplied to the soil A: Al ion was supplied to the soil (20 mM of Al ion solution was supplied to 16% of the soil), *AL* Al ion and lignin derivatives were supplied to the soil

and compared among different cases. The modified lignin was found to remove the toxic effect of aluminum ions and even improve the growth of the radish roots.

The second example of neutron imaging applied to the roots is the evaluation of water-absorbing polymers. In water-deficient areas, such as semiarid areas, how to keep water in the soil is a crucial problem, and sometimes special pottery containers filled with water are placed near the roots in the soil so that water gradually seeps out from the container and provides water to the plant for a considerable time. Therefore, water-absorbing polymers have attracted attention as replacements for such pottery containers. Since there are several kinds of water-absorbing polymers with different abilities to absorb water, two kinds of polymers were selected, and the method of supplying water from the polymer to the root was evaluated using neutron images.

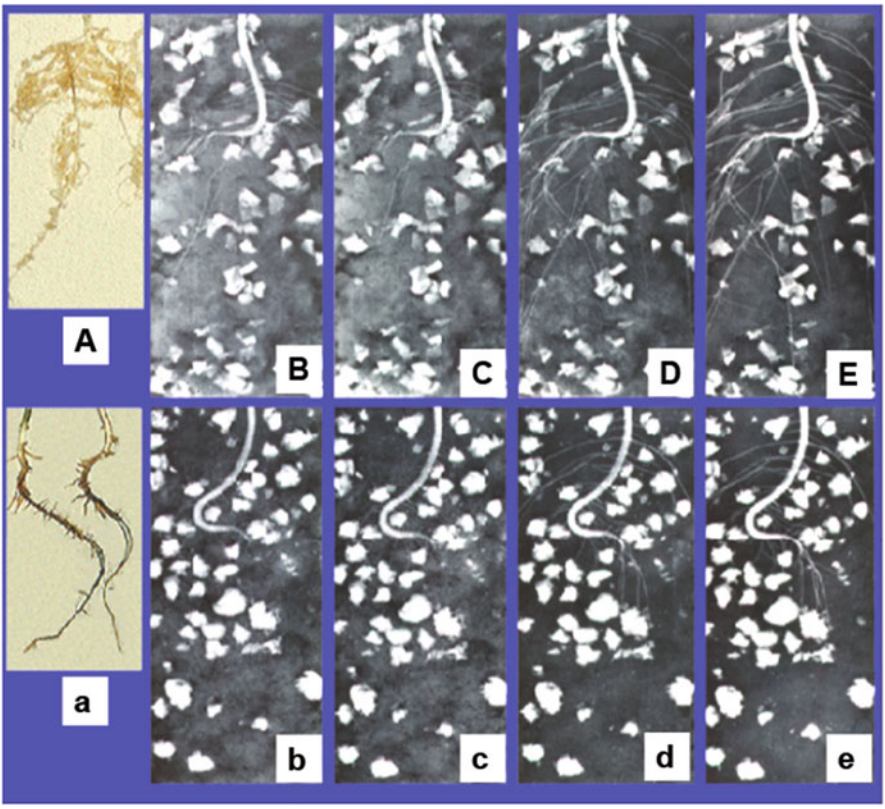

Fig. 1.8 Effect of two types of water-absorbing polymers on the soybean root development [4]. Two types of polymers were swelled in water solution and mixed with the soil: polyvinyl-alcohol polymer (**A**, **B**, **C**, **D**) and polyacrylic polymer (*a*, *b*, *c*, *d*). Then, soybean plants were grown in the soil mixture. In the case of the polyacrylic polymer, the water absorbed by the polymer was not supplied to the plant, and the color of the soil darkened with time, which indicates that the plant only absorbed water from the soil. The polyvinyl-alcohol polymer supplied water to the plants, and the image gradually faded. **A** and **B** are pictures of the roots grown in the container for a week

The neutron images of soybean root development in soil containing different kinds of water-absorbing polymer are shown in Fig. 1.8. The soybean seedlings were grown for 5, 6, 10, and 12 days in an aluminum container (150 × 70 × 3 mm) packed with soil containing polyacrylic water-absorbing polymer (*Acryhope*, Nippon Shokubai Kagaku Kogyo Co.) or polyvinyl alcohol copolymer (Mizumochi-ichiban, Nippon Gosei Kagaku Kogyo Co.). The white spots in the picture are the images of the polymers swelled with water. Therefore, the whiteness and size of each polymer showed where and how water was supplied from the polymer to the roots.

In the case of the polyacrylic water-absorbing polymer, as shown on the lower side of the images in Fig. 1.8, the size and whiteness of all the polymers were the same throughout the days of imaging, indicating that the water content in the

polymer was not changed. That is, the plant absorbed water only from the soil, and the water in the polymer was not supplied to the plant. Then, a shortage of water occurred, and the roots did not develop well. The length of the main root was approximately the same in all the images.

The upper images in Fig. 1.8 are neutron images of a soybean seedling grown in soil containing polyvinyl alcohol copolymer. At first, there is much water in the soil, in contrast to the observations of the polyacrylic polymer, where water in the soil was absorbed quickly from the first stage. Then, the size of the polyvinyl alcohol copolymers, especially around the upper part of the root, decreased with root development. When the color of the soil and the polymer was compared, first, the soil became darker, and then the polymers became darker and decreased in size. This phenomenon indicated that water was supplied first from the soil and then from the polymer. The side root was well developed compared to that in the polyacrylic polymer in soil. After neutron images were taken, the roots were removed from the container, and the state of the roots was compared. As shown in Fig. 1.8, the roots, including side roots, did not grow well, and the color turned dark when polyacrylic polymer was applied, whereas when polyvinyl alcohol copolymer was supplied to the soil, the roots firmly penetrated the polymer, indicating that the roots searched for water and absorbed water from the polymer.

1.2.2 3-Diimentional Images of Roots

To study the water absorption of the root in more detail, a 3-dimensional (3D) neutron beam image was constructed. The neutron beam image was a 2D image as long as the neutron beam came from one direction of the collimator. When many 2D projection images are taken, with neutron irradiation applied to the sample from different angles, 3D images can be constructed from many 2D images through computer processing. Therefore, the plant was fixed on a rotating table, and the angle of irradiation to the sample was varied. Many 2D images were taken, and then a spatial image was constructed through a computer.

1.2.2.1 3D Image Construction

A five-day-old soybean seedling was transplanted to an aluminum container (35 mm φ, 150 mm) packed with Toyoura's standard sand containing 15% (w/w) water. The soil surface was covered with aluminum foil to prevent water loss due to evaporation. The samples were kept at 26 °C under 70% humidity with 20,000 lux of light in a growth chamber and were taken out periodically for imaging. These procedures were the same as those to acquire 2D images using an X-ray film. The exposure was performed in a JRR-3 M research reactor installed at the Japan Atomic Energy Research Agency (JAEA). The neutron flux used for the exposure was 1.5×10^8 n/cm^2 s.

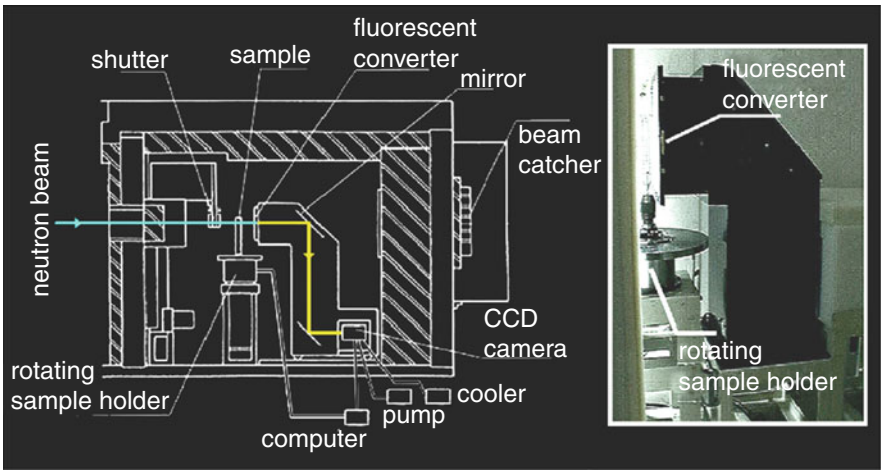

Fig. 1.9 Neutron irradiation chamber to acquire 3D image. Schematic illustration of the neutron irradiation chamber and a picture at JAEA. Neutrons were irradiated from the left-hand side, and the neutrons that penetrated the sample were converted to light by a fluorescence converter. The light beam was guided to a cooled CCD camera using two mirrors. The camera was shielded well with polyethylene and lead blocks. The sample was rotated by 180° in steps of 1°. The regulation of rotating the sample and the shutter speed of the camera were controlled using a computer

To obtain a CT image, the plant sample was set on a rotating disk (Fig. 1.9). The disk was fixed on a rotating table where a fluorescent neutron converter (NE426 equivalent made by Kasei Optonics Ltd.) was set as close as possible to the sample, at 2.2 cm from the rotation axis. The total neutron dose was 6.0×10^8 n/cm^2 per projection, and the L/D-value was 153. The shutter of a cooled CCD camera (C4880, Hamamatsu photonics, Co.) was opened for 4 s. The neutrons penetrating the sample were converted to photons by a fluorescent converter. The photon image was guided to the cooled CCD camera using two quartz mirrors. A MicroNikkor lens (F105 mm, Nikon Co.) was attached to the cooled CCD camera. The effective area of the fluorescent converter was approximately 5×5 cm. Since the CCD chip is very sensitive to scattered gamma-rays and neutrons, the camera was well shielded with polyethylene and lead blocks, each of which was $10 \times 10 \times 10$ cm. The sample was rotated in intervals of 1 up to 180°, and at each angle, a projection image was taken, i.e., 180 images were acquired for each sample to construct the CT image. The rotation of the sample and the shutter speed of the CCD camera were controlled by a computer. It took approximately 1 h to obtain 180 images, and each output image could be monitored on a computer. After neutron irradiation, approximately 1 h was needed to decay out the radioisotopes, mainly ^{28}Al (half-life: 2 min), produced during irradiation.

The size of the image transferred to the computer was 1000×1018 pixels. Then, each figure was corrected using two background images. One of the background images was taken when neutrons were absent (dark current), and the other was the image without the sample (shading). Therefore, at each image, dark current image

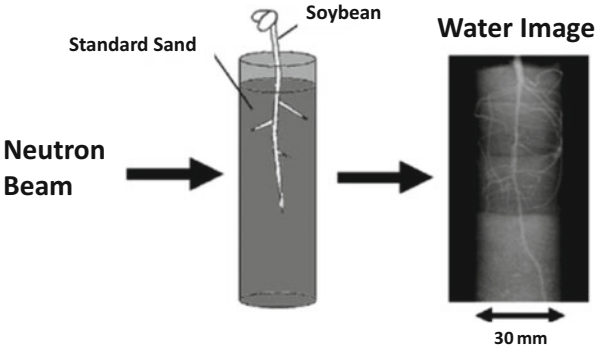

Fig. 1.10 Spatial image construction of a soybean root embedded in soil. A soybean plant grown in an aluminum pipe (30 mm $\phi \times 150$ mm) packed with soil was rotated by 180° in steps of 1°; at each angle, neutron imaging was performed. From 180 projection images, a spatial image was constructed using a computer

subtraction and shading correction were performed. Then, the root image, 600 × 1018 pixels, was cut out from the corrected figure to reconstruct the CT images. After sectional CT images were constructed at several root heights, sagittal CT images that included the main root were also constructed from a set of sectional CT images.

1.2.2.2 Water Movement Around the Root

Since plant development is slow, CT images can be used to evaluate the "static" spatial water distribution inside and around roots. The following is the spatial water distribution constructed from CT images in a soybean plant.

Successive neutron images of the soybean plant roots were taken during growth from 3 to 6 days. Each time, 180 projection images, acquired from different angles of irradiation to the sample, were processed on a computer to construct a CT image of the sample (Figs. 1.10 and 1.11). When successive sectional CT images at every pixel height were reconstructed and shown from the upper part to the bottom part of the container, they presented us with a basic question. Figure 1.12 shows the successive CT images. The main root is shown in the middle of all the images as a white spot, and whenever the side roots grow, they grow toward the wall of the container and then stop; therefore, the white dots at the wall are the tip of the side roots. The difference in the whiteness of the image showed the change in the water amount in the soil. However, it was always shown that surrounding the main root surface, shown in the middle, there was hardly any water. The root surface was always surrounded by a black area, indicating a water-deficient site.

Since there are no data on how much water exists at the surface of the root, especially within 1 mm of the root surface, the neutron images shown in Fig. 1.12 were of considerable interest. The evidence of the images that there is hardly any water adjacent to the root surface raises many questions about the water absorption activity of the root itself. How does this phenomenon happen? It is widely known that the composition ratio of the soil matrix, air, and water in cultivated soil for farming is approximately 1:1:1. Too much water in soil is harmful to plant growth.

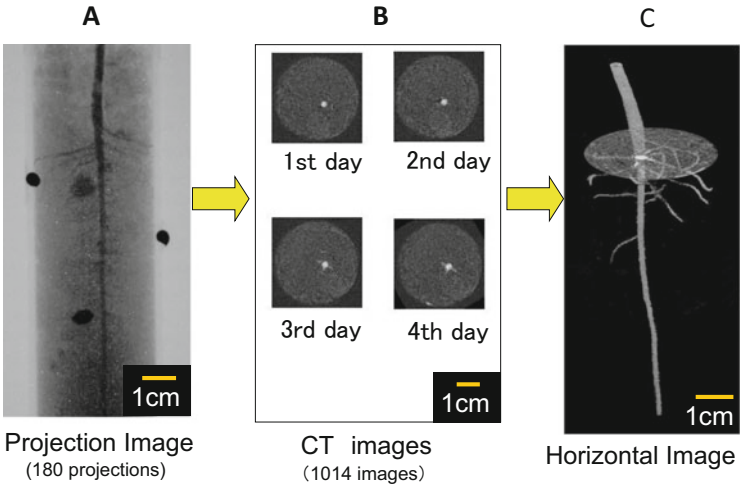

Fig. 1.11 Neutron images and root growth. (**a**) projection image of a control soybean sample on the 4th day (1014 × 510 pixels). The whiteness in the figure corresponds to the water amount. Black dots in the image are cadmium standards to adjust the position at CT construction. (**b**) CT images at the same height of the container during 4 days: the large white spot at the center indicates a main root

Roots absorb water from the soil, but why does hardly any water exist immediately adjacent to the root surface?

One of the answers is that growing roots perform movement, called circumnutation (see Chap. 8). Therefore, roots are always searching for favorable conditions in soil to grow, not only for nutrients or water but also for favorable physical conditions of the soil, hard or soft. Because of this movement of the root, the soil around the root tip is put aside during growth, and as a result, a small space is created around the root tip that seems to facilitate growth.

By stacking the dissection images taken every 50 μm, a 3D image of the water and the root imbedded in the soil was constructed. Figure 1.12 shows the CT image of the root imbedded in soil and the 3D image when approximately half of the area of the horizontal CT images was superposed, showing the root.

The whiteness in the image was calibrated well to the water amount. The calibration curve of the whiteness in the figure to water amount is shown in Fig. 1.13.

To visualize the decreased water in the soil more clearly, six reconstructed CT images corresponding to different heights of the container were superposed sequentially on the root image, which was taken from the 3D image of the whole container. These images permitted the comparison of water content changes during growth (Fig. 1.14). Figure 1.14 shows that within a few days, the amount of water in the upper part of the container decreased, corresponding to increased root formation. As shown in the figures, the water holding capacity near the root shifted downward with root development, suggesting movement of the active site in the root. The line profile of the whiteness in the soil along the main root showed that when the side roots were

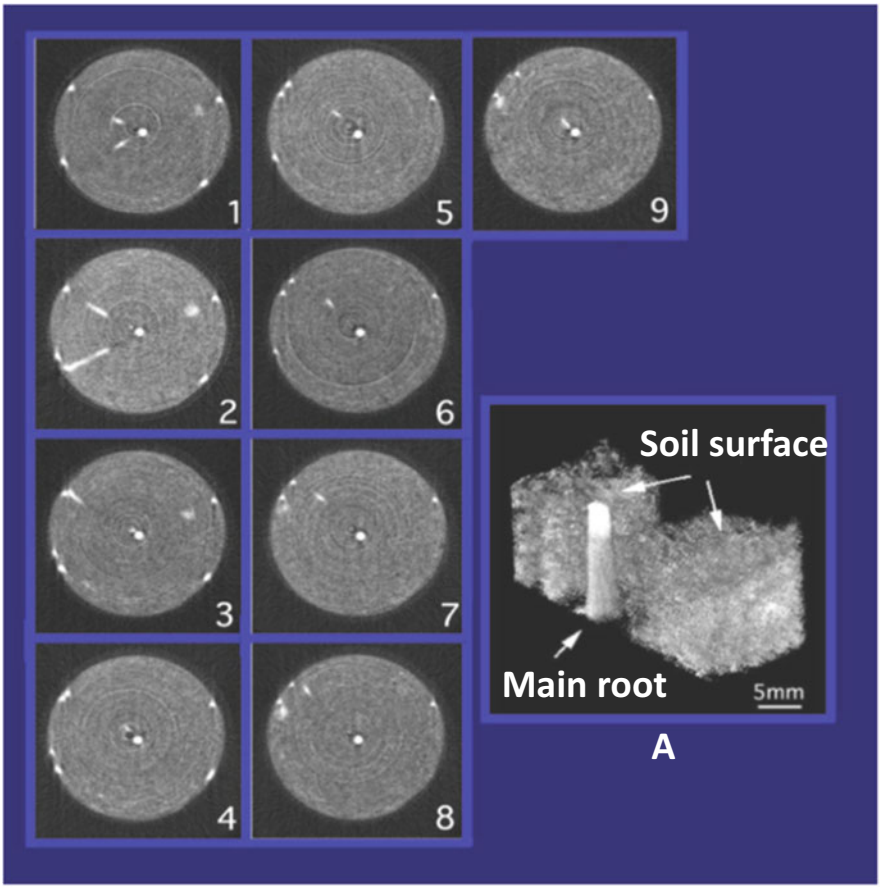

Fig. 1.12 CT images and upper part of the container [2]. From 180 projection images, CT images were constructed. The left figures show the successive CT images constructed every 1 mm from the upper part of the soil to the bottom (1–9). The white spots in the middle show the main root, and the radial white images from the center towards the wall of the container are the side roots that stop at the wall of the container. In most images, there is no water in the neighboring site of the main root, as indicated by the black color, which suggests that the root was absorbing water vapor, not water solution. **A:** spatial image produced by superposing half of the successive 400 CT images, which were taken every 50 μm, at the upper part of the container

about to emerge, the amount of water at those sites decreased (data not shown). When the water profile in the soil was calculated, there was a minimum in the water gradient near the root, approximately 1.0 mm from the root surface. Then, from this point, the water amount sharply increased toward the surface. The root surface was highly wet with more than 0.5 mg/mm^3 of water but not saturated. When Al (10 mM) was applied to the soil, root development and the water holding activity of the root decreased (data not shown).

From the tomographic root images, the position and lengths of the side roots, as well as water movement around them, can be quantified. When the whiteness of the

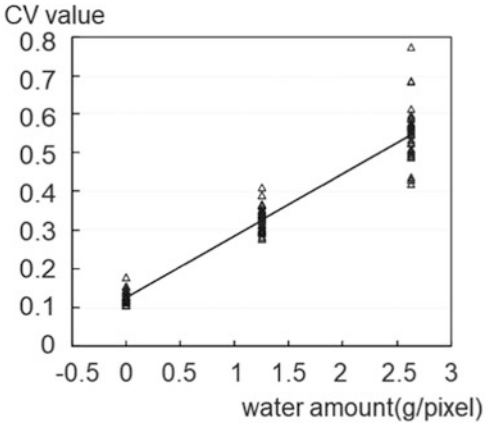

Fig. 1.13 Calibration curve to convert the whiteness value (CV) to water weight (g) [5]. Three standard samples containing 0, 10, and 20% water were measured. Five 10 × 10-pixel areas from 6 CT images were used in each standard sample. Therefore, 30 areas of whiteness were plotted for each sample. The calibration curve was obtained from an average value in each sample

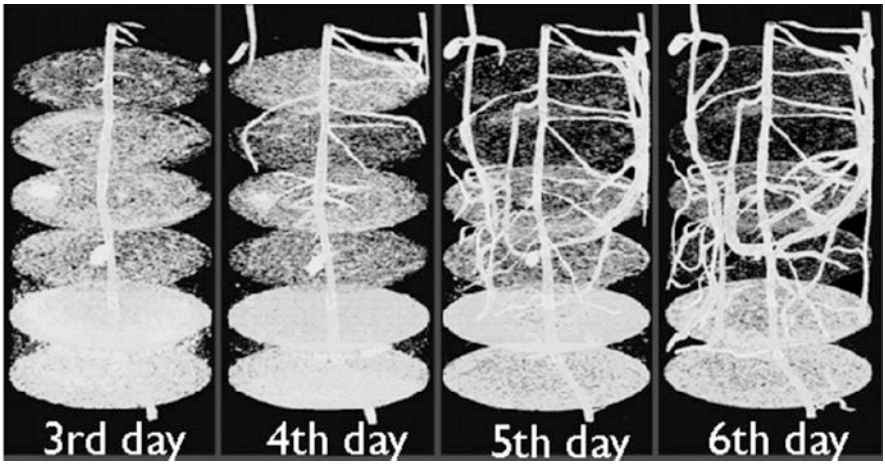

Fig. 1.14 Spatial root development with 6 CT images [6, 7]. After piling up all CT images, the spatial root image was obtained through image analysis. Six CT images constructed at different heights of the container were superposed to the root images. The whiteness in the CT images enabled us to compare the changes in water content. Within a few days, the amount of water in the upper part of the container decreased, which corresponds to an increased formation of roots

3D neutron image within 10 mm of the root was removed, the relative decrease in water amount near the root during root growth could be plotted (Fig. 1.15). The successive neutron images also provided information on side root growth, namely, the length and the emergence sites of the side roots, from which position they initiated their growth.

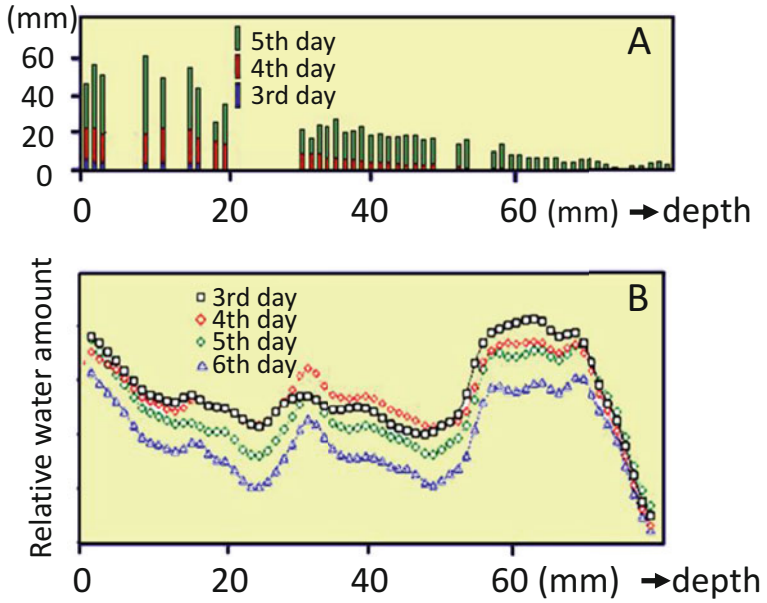

Fig. 1.15 Side root growth and water amount [6, 7]. Quantitative measurement of side root growth according to their position along the main root and water distribution around the main root days after watering the specimen. (**a**) Side root growth and position, (**b**) Water amount along the main root. Depth in mm

There was an obvious increase in side root growth around the upper part of the container (up to 20 mm down from the air/soil interface) compared to side roots located farther down the container. This correlates to a decrease in the water amount found in the soil. However, from this interval of imaging, it was difficult to know whether the decrease in water around the root was due to the horizontal movement of water or to vertical movement along the main root, since water deficiency in some region drives the movement of water toward this site.

Root surfaces and volumes were also calculated from the neutron images. The toxicity of Al ions was analyzed from these calculations since, as previously noted, the presence of aluminum ions is one of the main factors inhibiting plant growth in acidic soil. When 10 mM $AlCl_3$ solution was applied to the soil where a soybean seedling was growing, both the root surface area and root volume decreased [8]. The toxicity of the heavy metal was also visualized by the morphological development of the roots; an example is shown above in Fig. 1.7.

Since neutron imaging has a wide range of effective applications, we tried to apply this technique to other fields. One is fertilizer development, especially in the case of capsule fertilizer, where nutrients seep out gradually during growth (data not shown). Another promising application of this imaging is to study the relationship between root development and yield. It is empirically known that plants with high yield also have well-developed roots. To support this phenomenon with scientific

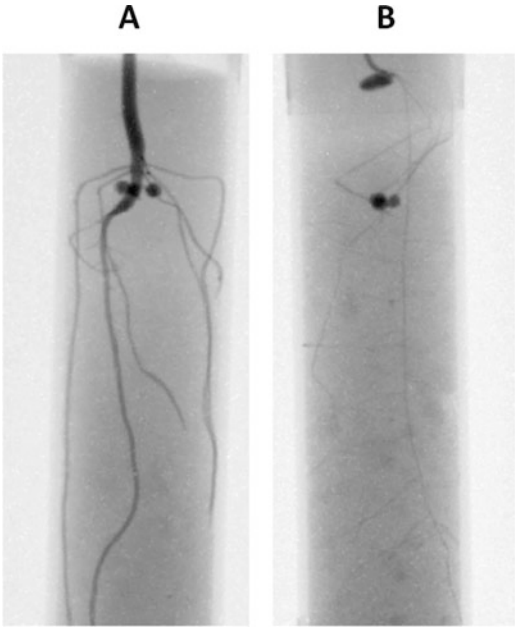

Fig. 1.16 3D images of roots embedded in soil. *Black dots* are cadmium standards to adjust the position at CT production. (**a**) Soybean root, (**b**) Wheat root

evidence, further study as to determine how water or fertilizer application promotes growth is desirable, since how to increase crop yields is an important issue all over the world.

Last, as an example of the 3D imaging of roots, spatial images of the soybean and rice roots grown in an aluminum container are presented in Fig. 1.16, where all the CT images were superposed sequentially, from the bottom to the top of the container. Even the fine secondary roots, especially in the case of the rice plant, are clearly shown.

The water profile around the root is not well known since methods of water measurement in small areas of the soil have not been well developed. In field studies, a lysimeter has been used to analyze the moisture balance in the soil, supplying water to the restricted area, and the changes in water amount due to evaporation along with the soil weight were analyzed for calibration. More specifically, water sensors were inserted into soil at certain intervals from the root, and the water amount at the surface of the root was calculated by extrapolating the water profile measured from the sensors, assuming that there was a gradient of water amount toward the surface of the root.

There is no other method comparable to neutron beams to image the water absorption activity of a living root imbedded in soil. Since the roots are the basic tissue that supports plant activity, nondestructive visualization of the morphological development of the roots and of water absorption has a high potential to be applied not only for physiological research on plants but also to the in situ analysis of plants grown in the field.

1.2.3 Water Images of Flowers

When neutron imaging techniques were applied to plant research, first, this method was mainly employed to analyze the aboveground portion of a plant. For example, neutron imaging of a cowpea plant revealed the role of special internode tissue, whose function was to store water (see Chap. 2, Sect. 2.2). Under water-deficient conditions, water is primarily moved from the internode to other tissues. The neutron imaging method was further developed to measure the amount of water actually moving in an internode using ^{15}O-labeled water (see Chap. 2, Sect. 2.3).

One of the reasons neutron imaging was applied to the above-ground part was that it was relatively easy to take the image by simply placing the sample between the outlet of the neutron beam and an X-ray film. As shown in Fig. 1.17, the plant sample was set vertically in front of the cassette in which the X-ray film was placed in vacuum and was irradiated with a neutron beam, by the same method described above for root samples. Figures 1.18, 1.19, and 1.20 are examples of neutron images of flowers: tulip, rose, and convolvulus, respectively. The whiteness in the figure corresponds to the amount of hydrogen in the sample. As mentioned above, at the introduction of neutron imaging, the whiteness could be regarded as an image of the water in a living plant since more than 80% of plant tissue consists of water. Whiter regions indicate the water-rich regions, and the change in whiteness during the treatment indicates the change in the water amount.

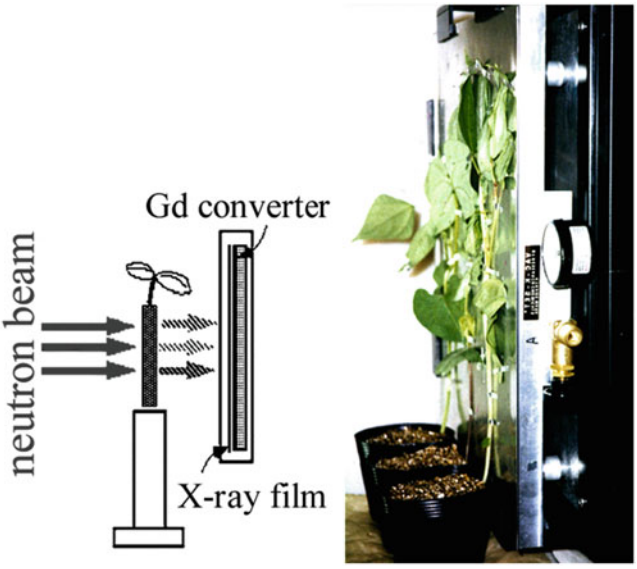

Fig. 1.17 Neutron beam imaging for the aboveground part of the plant. The sample was placed vertically in front of the cassette where the Cd converter and an X-ray film were sealed in vacuum. The neutron beam was irradiated to the sample, and the neutrons after penetrating the sample were converted to β-rays to produce the image on an X-ray film in a cassette

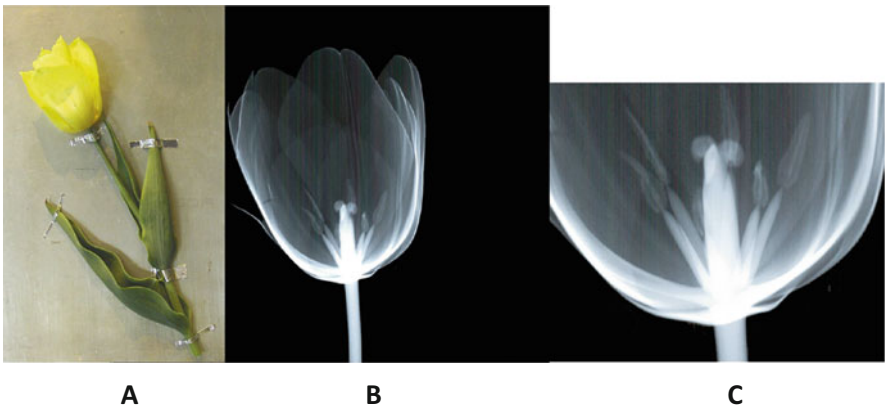

Fig. 1.18 Water image of a tulip flower by the neutron beam. The degree of penetration of the neutron beam highly depends on the amount of water in the sample. The whiter part indicates higher water content. The neutron beam cannot penetrate the site with high water content; therefore, the exposure of the X-ray film with converted radiation from neutrons behind the plants was low, which resulted in a whiter image. Through calibration, the amount of water in the tissue can be obtained. (**a**) picture of the tulip flower; (**b**) neutron image of the tulip flower; (**c**) magnification of (**b**)

Fig. 1.19 Water image of a rose flower by the neutron beam

As an example of water analysis in a cut flower, a rose image is introduced. An important issue in the cut flower industry, especially for roses, is how to extend the flowering stage. In the case of a rose flower, sometimes the "bent neck" phenomenon occurs during the shipping of the cut flower. Once this phenomenon occurs, the bent neck never returns to the straight position and withers. The bending phenomenon always occurs at the stem, very close to the bottom part of the flower, and was hypothesized to be induced by water deficiency at this part of the stem. To determine from which regions the rose flower loses water, neutron imaging was employed.

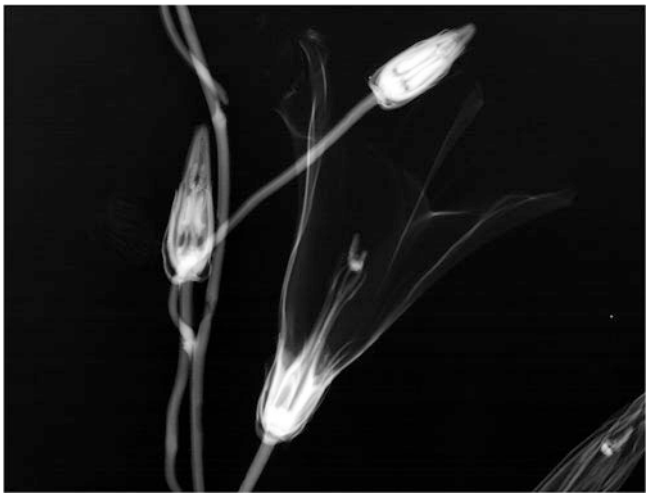

Fig. 1.20 Water image of a convolvulus by the neutron beam

Fig. 1.21 Rose flower images before and after the bent-neck phenomenon. (**a**) Picture of rose flowers; (**b** and **c**) Water image of rose flowers before and after the bent-neck phenomenon. Under dry conditions, the water amount in the internode decreased and could not support the flower part to remain straight, so the flower part was bent

Figure 1.21 is a picture of cut rose flowers and neutron images of these flowers before and after the bent neck phenomenon occurred. To take the neutron image, flowers were fixed on an aluminum board with aluminum tape, as shown in

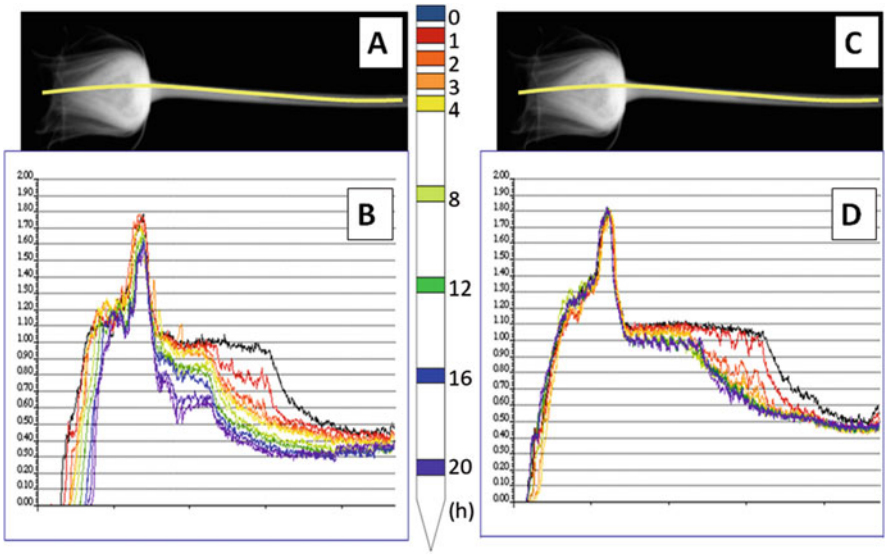

Fig. 1.22 Water amount in a cut flower of rose. (**a**) Water image of a rose flower acquired during the drying process; (**b**) Water image of the rose flower when water was supplied after the drying treatment. The line profile of the water amount was plotted after 0, 1, 2, 3, 4, 6, 12, 16, and 20 h of treatment. Different colors according to time were added to the line profile

Fig. 1.22. When the bent neck phenomenon occurred, the stem had become thinner with less water.

To analyze the water decrease in more detail, neutron images of the flower were taken after 1, 2, 3, 4, 8, 12, 16, and 20 h of the drying process. Before the drying treatment began, 0 h, the water content in the cut flower was very high at the bottom part of the flower and the upper part of the stem, close to the flower. The bending phenomenon occurs at this part of the stem, which initially contained a high amount of water compared to the lower part of the stem. The water content at this site of the stem was maintained well during the first several hours of drying treatment. However, after 8 h, the water in this part gradually decreased.

Next, after 4 h of drying treatment, when the water in the upper part of the stem was not decreased dramatically, water was resupplied. By supplying water again from the bottom part of the stem, the decrease in water at the flower ceased, and water was gradually restored in the stem. However, water was hardly restored at the highest part of the stem close to the flower. The result that water was not reabsorbed at this site in the stem suggested that this site has a special function in maintaining the flowering stage.

That is, when drying conditions began, this part was resistant to decreasing water; however, once water had decreased, water was hardly restored to this part of the stem. This feature might indicate a plant strategy for survival under drying conditions. It seems to require much energy to proceed to the seed ripening stage after the senescence of the flower. Therefore, when the surrounding conditions were not

favorable for the plant to develop seeds, such as under low-water availability, the plant could stop the ripening process by discarding the flower part. Bending the higher part of the stem allowed the plant to spend less energy on further development for seed production. However, this example of neutron imaging of cut flowers involves some speculation.

Extension of the life of cut flowers is a key issue in the floral industry, and the amount of water in a flower plays a key role in maintaining its flowering stage. Neutron imaging of cut flowers showed detailed images of water content in flowers such as lilies, morning glories, and carnation. The next is the case of carnation cut flowers, where some attempts were made to extend the flowering stage by supplying modified water. The viscosity of the water was increased by dissolving Xe gas under high pressure, and the prepared water was supplied to a carnation flower to determine whether it helped to prolong the life time of flowering after it was harvested. To acquire the neutron image of the flower, the flower part of the carnation was wrapped softly with aluminum foil, and 180 projection images were taken in the same way as for the root sample. Then, a 3D image of the carnation flower was constructed from the projection images, and the effect of modified water was analyzed by comparing the sagittal images produced. First, the 3D images of a carnation flower demonstrated the importance of water inside the ovule to maintain the flowering stage (Fig. 1.23). The application of water containing dissolved Xe gas to a cut flower helps to control the metabolism of the flower, slowing the deterioration process mediated by an enzymatic reaction (Fig. 1.24).

1.2.4 Water Images of Wood Disks

The green moisture in a wood disk image was shown for the first time by neutron beam irradiation. Image analysis also showed how moisture in wood disks is decreased during the drying process.

There are several features of moisture distribution in the trunk of Sugi (*Cryptomeria japonica*), which is a popular wood utilized in housing materials in Japan. In many cases, there is a so-called white zone at the inner part of sapwood adjacent to the heart wood, recognized by its whiter color. The white zone consists of several annual rings and contains less moisture than surrounding tissues. Green moisture content, especially in heartwood, differs drastically among cultivars or even among individual trees of the same cultivar. It is not known what causes the difference in green moisture content in heartwood, genetics or environmental conditions where it grows. It was reported that there is a reciprocal correlation between the darkness of the color tone and the moisture content in heartwood, where with increasing moisture content, the color becomes darker. Until the tree is cut down, it is not known whether the moisture content of the heartwood is high. Therefore, it is important to distinguish trees with lower or higher moisture content in the heartwood before cutting them down.

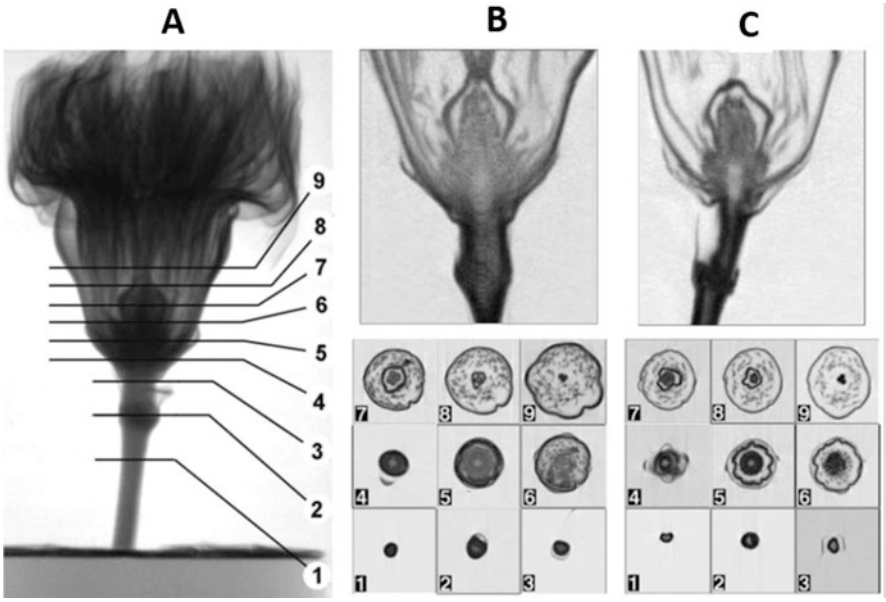

Fig. 1.23 Three-dimensional water image of carnation flowers [9]. Carnation flowers were wrapped with aluminum foil and rotated during neutron beam irradiation similarly to the roots embedded in soil. When all cross-section images constructed at every 50 μm interval at height were obtained, they were superimposed to construct the three-dimensional water image. The lower part of the flower (2 cm) was selected, and transverse sections at each height are shown. (**a**) 3D image of the flower; (**b** and **c**) Cross-section images at nine heights indicated in A before and after the drying treatment, respectively, where the plant was kept under 30° in a phytotron for 2 h without water supply

When the green moisture content in heartwood was high, drying took longer. Since residual moisture after drying lowers the quality of the lumber, eliminating moisture completely from the heartwood is one of the serious problems in kiln drying. To study the decrease in water during the drying process, four cultivars of Sugi, 24-year-old 25-Gou, 25-year-old Honjiro, 29-year-old 1-Gou, and 30-year-old Sanbusugi were cut down in the University Forest in Chiba, Faculty of Agriculture, The Univ. of Tokyo. Approximately 60 cm of the log at breast height was removed by a chain saw, and each end of the log was sealed tightly with vinyl sheets to prevent moisture loss due to evaporation. The next day, the logs were taken into an atomic reactor, JRR-3 M, installed at Japan Atomic Energy Institute, and cut further to obtain wood disks approximately 1 cm in thickness immediately prior to neutron irradiation. The diameters of the disks were 16.6, 8.4, 8.6, and 13.7 cm for 25-Gou, Honjiro, 1-Gou, and Sanbusugi, respectively.

The disks were fixed on an aluminum cassette by aluminum tape where a gadolinium converter (25 μm in thickness) and an X-ray film (Kodak SR) were sealed in vacuum. The cassette with samples was set perpendicular to the neutron beam and irradiated for 19 s. Ten minutes was needed to cool down the sample.

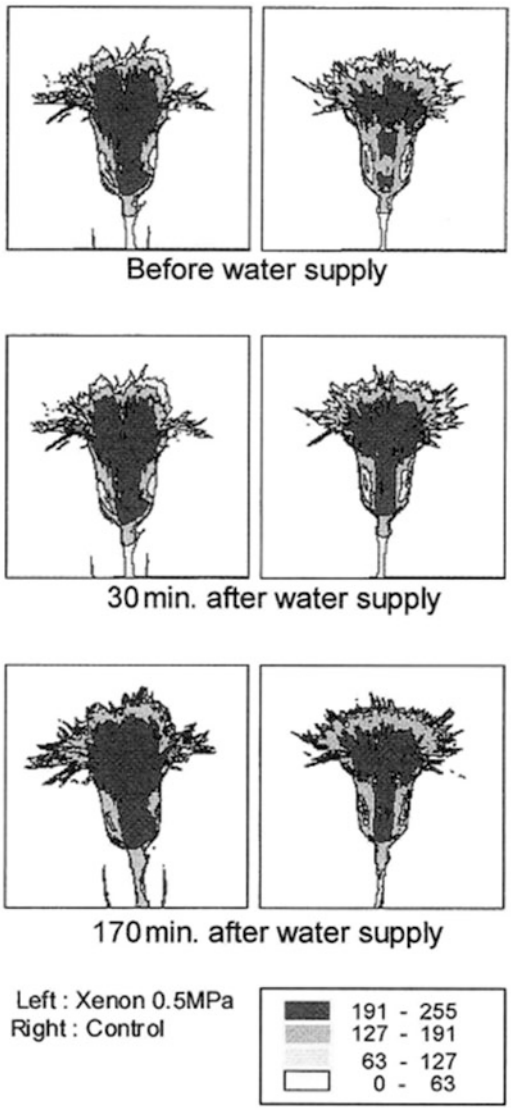

Fig. 1.24 Water images in the carnation flower when Xe-gas-dissolved water was supplied [10]. 2D-neutron images of a carnation flower after being supplied with water containing xenon. The *darker* areas indicate water-rich parts. The xenon in water maintained a higher water amount; therefore, the flowering stage was maintained longer in the cut carnation flower

After irradiation, the wood disks were kept in a phytotron at 60 °C with 90% humidity to reduce the moisture in the disk. During this drying treatment, the wood disk was periodically removed from the phytotron, and neutron irradiation was performed in the same manner as described above. Then, the X-ray film was developed carefully, and the image on the film was transmitted to a computer through a CCD camera (Hamamatsu Co, 2330).

Figure 1.25 shows the picture and corresponding neutron image of wood disks of four cultivars. In the neutron images, a whiter color indicated regions where green

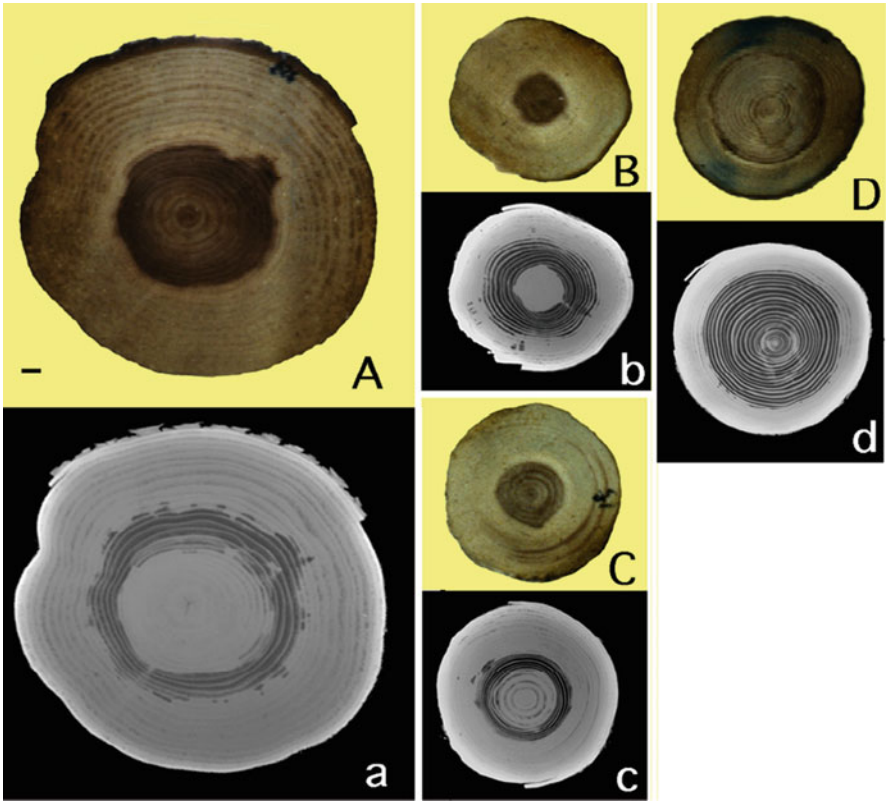

Fig. 1.25 Water image of a wood disk of the cedar tree, Sugi [11]. Optical pictures and neutron images of four cultivars of Sugi (*Cryptomeria japonica*), 25-Gou (**A**, *a*), Honjiro (**B**, *b*), 1-Gou (**C**, *c*), and Sanbusugi (**D**, *d*) before drying. The upper figures for each type (**A**–**D**) are photographs of the sample disks, and the lower figures (*a*–*d*) show the corresponding neutron images. The *bar* indicates 1 cm for all figures. The *darkness* in the neutron image corresponds to the degree of moisture deficiency

moisture content was higher. The darkness in the image showed the extremely low moisture content in the intermediate zone between heartwood and sapwood in most of the cases. Within one annual ring, the neutron image showed a regular moisture distribution pattern, both in heartwood and sapwood. Therefore, tracing the moisture-deficient zone that appeared repeatedly throughout the disk enabled us to know the position and number of the annual ring. Among the four cultivars, 25-Gou (a) and Sanbusugi (d) showed the highest and lowest water content in the heartwood, as revealed by the color tone in the neutron images, (A) and (D), respectively. As noted above, it is empirically known that when the color of the heartwood is dark, the moisture content tends to be higher, which was consistent, as shown in Fig. 1.25.

Since the residual moisture in lumber after drying is the largest problem in the utilization of Sugi as a material, two cultivars with different water profiles, as shown

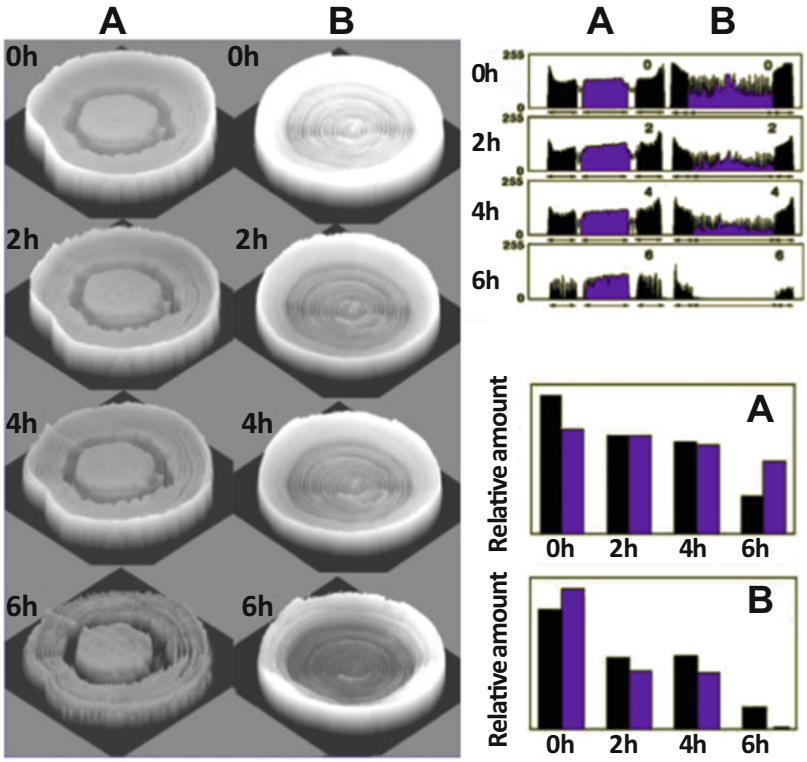

Fig. 1.26 Water image of the cedar tree during the drying process [11]. Wood disks of cedar trees, which were 1 cm thick, were removed every 2 h during the drying process, and neutron images were obtained. The 2D neutron images were converted to 3D images of the wood disk where the height of the image corresponds to the relative moisture content. The *upper-most figure* shows the green moisture pattern, and the downward successive images indicate those after 0, 2, 4, and 6 h of drying treatment. (**a**) and (**b**) correspond to 25-Gou and Sanbusugi, respectively. *Upper right*: Water profile along the line, including the center, across the neutron image of the disk. *Lower right*: relative water amount at the heart wood and sap wood of the area in the line profile of the wood disk at fight high. *Purple region*: heart wood; *Black region*: sap wood

in Fig. 1.25, were chosen, and the changes in water content and profile in the wood disks during the drying process were studied by neutron imaging. The samples were kept in a phytotron at 60 °C with 90% humidity. Every 2 h, the wood disk was removed, and a neutron image was taken. Figure 1.26 shows the neutron images of 25-Gou and Sanbusugi, which, respectively, had the highest and lowest water content in heartwood among the four cultivars, taken during the drying process. The 2D neutron images shown in Fig. 1.25 were converted by a computer to produce 3D images in which whiteness in the image corresponded to the height, so that the higher regions represented water-rich regions. Then, the line profile of each image across the middle was taken out to show the dissection image of water in the disk. The pattern of decreasing moisture on the plane of the disk showed that the moisture

of the heartwood tended to remain at a higher level in 25 Gou. The water decrease during the drying process was also clearly indicated when the heartwood area in the dissection image was plotted to show the relative change in the water amount in the disk.

The results can be summarized as follows. In short, when the water content in heartwood was high, the color tone of the heartwood in the neutron image was whiter, and the water amount in the heartwood remained high during drying treatment, whereas when the water content in the heartwood was low, shown by a darker color in the image, the water in heartwood was more easily lost during the drying treatment. The main part of lumber utilized for manufacturing is the heartwood, and water remaining in the wood after manufacturing will induce fractures or cracks during years of usage. However, there is no information about what causes the difference in water amount in heartwood. Indeed, even neighboring trees of the same cultivar showed different water content in the heartwood; the water content was known only after felling the trees.

To obtain additional water images of trees, several kinds of trees grown in the University Forest were felled, and logs 80 cm in length were prepared from a portion at approximately breast height 4 h before neutron imaging was performed. Special care was taken to cover the surface of the log to prevent water loss before preparing the disk for imaging. Then, the wood disks were prepared immediately prior to irradiation and irradiated with a neutron beam, by the same method described above for Sugi. From the images taken, two kinds of trees with interesting water profiles are presented in Fig. 1.26. These images represent wood disks (1 cm in thickness) of metasequoia (*Metasequoia glyptostroboides*) and Japanese cypress (*Chamaecyparis obtusa*), which were 10 and 19 years old, whose sizes were 13.2 and 12.3 cm in diameter, respectively. Similar to the neutron images of Sugi, there was a repeating pattern of white areas in the disk indicating the annual rings. In the case of metasequoia, although there was no color change observable in the picture taken by a camera, the neutron image showed a clear difference in water distribution. The outer several rings contained much higher amounts of water, whereas the water content in the center part was low. The distribution pattern of water within the disk suggested that heartwood formation had already started with no change in the color tone (Fig. 1.27).

In the case of the cypress, white color, indicating a water-rich part, was observed, especially at a few outer annual rings. However, from place to place, the water-rich part penetrated a few annual rings. It was interesting that there was no rigid border for water distribution, i.e., water was not confined within one annual ring but seemed to move across the annual rings. If this image indicated water movement across the annual rings, many questions arose. Since there are many ions dissolved in water, the ions could move with water. The movement of ions indicates information movement associated with water movement. The transfer of information across the annual rings suggests that there is another activity within the heartwood and sapwood, information transfer. There is a method to measure the age of the trees by analyzing ^{14}C activity in the carbon contained at a specific annual ring. Since the decrease in ^{14}C activity correlates well with the number of annual rings actually counted, it seems

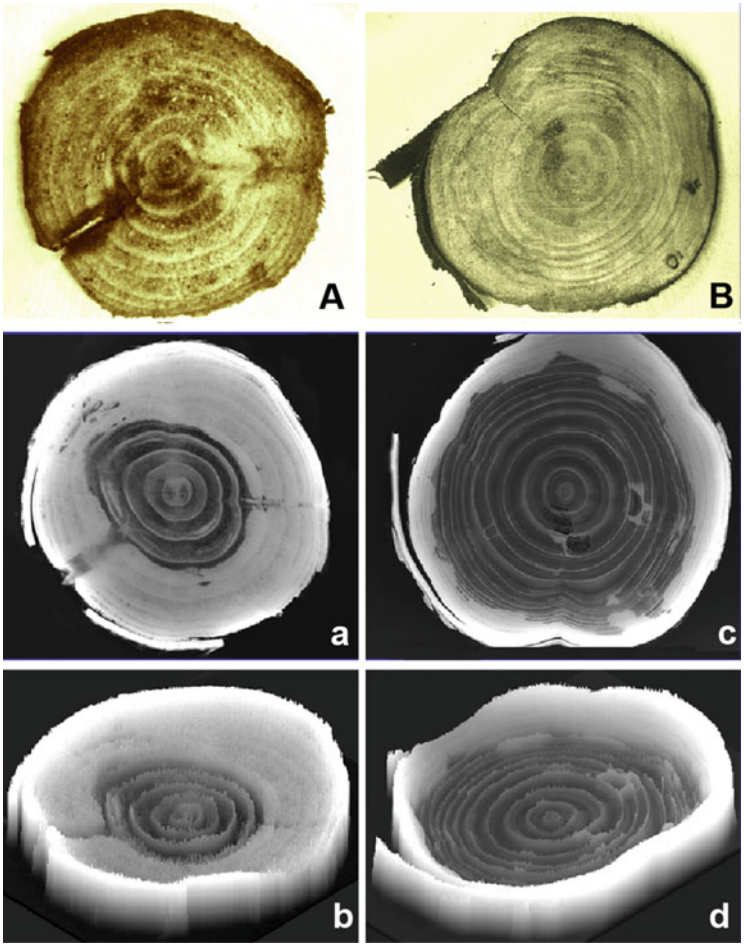

Fig. 1.27 Water image of metasequoia and Japanese cypress. Water images of the wood disks (1 cm in thickness) of metasequoia (*Metasequoia glyptostroboides*) (**A**, *a*, *b*) and Japanese cypress (*Chamaecyparis obtusa*) (**B**, *c*, *d*) are shown. **A** and **B**: Photographs of disks. The 2D neutron images (*a*, *c*) were converted to 3D images (*c*, *d*) by a computer where the height corresponded to the water amount, which is the whiter part in the 2D images

that the carbon structure in the trunk hardly moves, and only water moves in the structure of the carbon network created within the trunk.

We always wondered why most of the tissue in a tree consisted of dead cells. Most living cells exist, particularly in the outer layers of the trunk, and proliferate to enlarge the structure. To maintain the structure of the trees, large amounts of tissues are needed to produce hard trunks. However, when all tissues consist of living cells, they require a large amount of nutrition and energy. The most efficient way to support the structure might be that most of the trees consist of dead cells that do

not require energy. However, information must move within the tree, such as to decide when to start the formation of heartwood or to enlarge the heartwood volume.

All the cells in the layer surrounding the heartwood in the sapwood should become dead cells to join the heartwood year by year. It is known that a few percent of the cells in sapwood are alive. When the heartwood increases, how these cells in sapwood, next to the heartwood, become dead cells is not well understood. Are the few living cells in sapwood killed at the border with the heartwood? Although we are apt to focus on the activities of living cells to study plant activity, the role of dead cells might be taken into account.

Important aspects of the physiological activity of a tree could rely on knowing the water and element distribution inside the wood. However, another perspective is to study the element distribution within a tree. We investigated the element distribution within a tree grown in a tropical rainforest, where annual rings were not formed because the weather is relatively constant throughout the year. Through activation analysis of the elements, the distribution of the ion concentration within the disk showed each ion-specific gradient or pattern (data not shown), suggesting that the transmission of each ion might have a specific role in the trunk; therefore, it seemed that there was specific information transfer activity within the tree trunk.

1.2.5 Water Images of Seeds

What kind of image can be taken when seeds are irradiated with neutron beams? Figure 1.28 is a neutron image of corn seeds at an early stage of germination. As shown in the figure, the water distribution within the seed is not uniform, and there is always a water-rich part that will grow as a root to develop toward the outside of the seed.

To visualize how seeds absorb water from outside and how water moves or accumulates in the seed to germinate, water absorption images of the seeds were taken. Five seeds were prepared for neutron irradiation during the water absorption

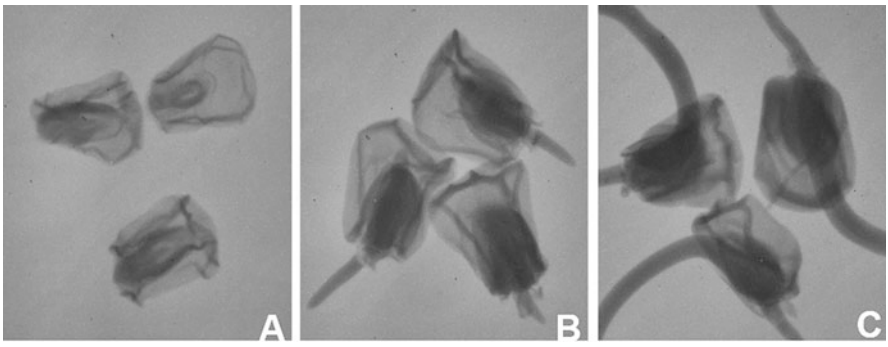

Fig. 1.28 Water images of corn seed germination

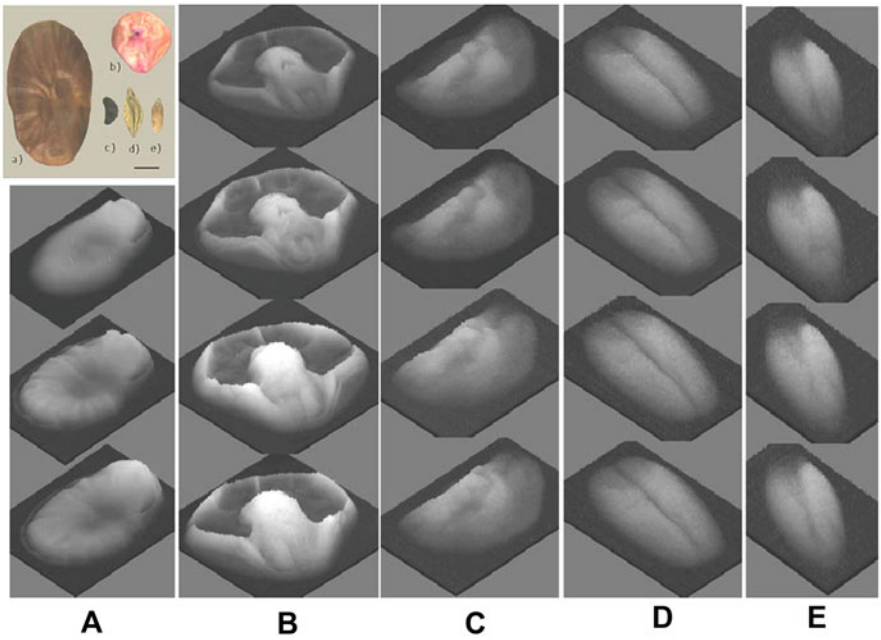

Fig. 1.29 Water absorption process of seeds [12]. Three-dimensional neutron images of the seeds during the water absorption process are shown from top to bottom. Five types of seeds were dipped in water: broad bean (**A**, *a*), corn (**B**, *b*), morning glory (**C**, *c*), wheat (**D**, *d*), and rice (**E**, *e*), and neutron imaging was performed after 1, 2, and 3 h. In the case of the broad bean, the images before and after 1 and 2 h of water treatment are shown. The height in the image represents the water amount, i.e., the whiteness in the image. The standard sample was simultaneously irradiated to normalize the whiteness of the image taken at different stages of water absorption. The distribution of water after absorption was not uniform in all seeds. Water preferentially accumulated at the embryo site in seeds. *Upper left*: photograph of five seeds. The *bar* indicates 5 mm

process: broadbean (*Vicia faba* L.), corn (*Zea mays* L. cv. Kou 504), morning glory (*Ipomoea nil* L. cv. Murasaki), wheat (*Triticum aestivum* L. cv. Minorimugi), and rice (*Oryza sativa* L. cv. Norin 61). The seeds were dipped into water, and after 1, 2, and 3 h, they were removed from the water and wiped well to remove the water remaining at the surface of the seeds. Then, the seeds were fixed on an aluminum cassette where an n/γ converter and an X-ray film were sealed in vacuum. The neutron irradiation of the seeds was performed repeatedly in the same way used for the other samples cited above. To visualize the water distribution within the seeds more clearly, the 2D seed image was converted to a 3D image, where the height indicates whiteness, that is, the amount of water.

As shown in Fig. 1.29, the whiteness in seeds increased with increasing water amount in seeds, but the increase was not uniform. There seemed to be a specific route for water to move within the seeds. In the case of broad bean (a) and corn (b), the water amount was especially high in the embryo. However, in the case of wheat (d) and rice (c), water uptake was found to be higher at the endosperm. Swelling of

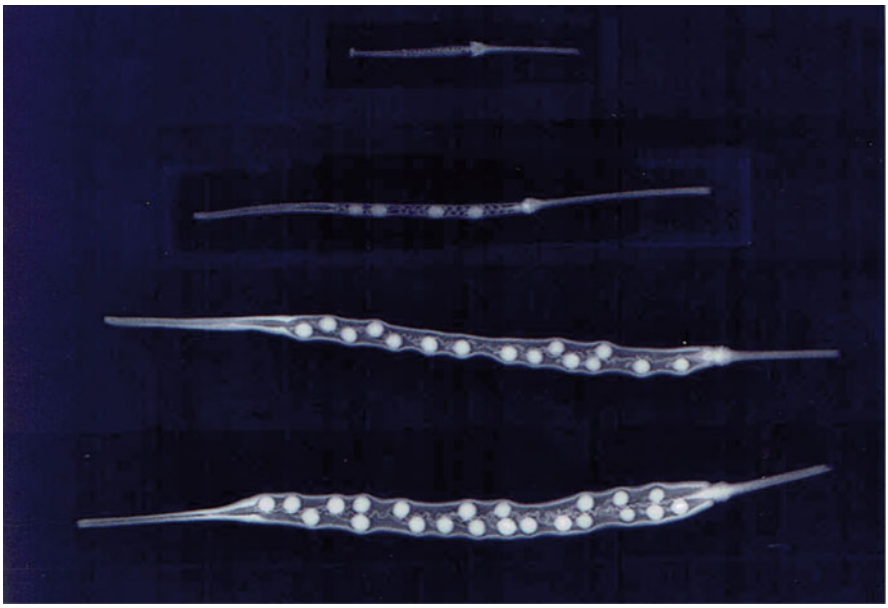

Fig. 1.30 Water images of the rape plant pods [13]. The rape plant pods after 7, 14, 20, and 27 days of flowering from top to bottom

the embryonic root and shoot was clearly observed in the morning glory (c). Since the neutron images showed only the distribution of the water amount and not the route of water movement, it was not known how the water actually moved within the seeds. Several kinds of water channels, aquaporins, are reported in plants; are there many kinds of aquaporins working at different sites in the seeds at different times? Another question regards the subsequent stages of germination. For example, it is not known how the seed skin is triggered and which part of the seed skin opens to allow the root to emerge from the seed. How water moves within the plant could provide some clues to answer such questions.

Several rape plant pods (*Brassica naps* L.) were harvested at different developmental stages of seed formation, and neutron images were taken, since a pod is an important tissue where the optimum conditions for seed development are created. During the ripening of the pod, the water content of the seed reached a maximum at approximately 20–30 days, at an early stage, and then began to decrease, whereas the weight of each seed gradually increased throughout the ripening process because of oil formation. Therefore, there should be a drastic change in chemical transport through the vascular system during the ripening process, including limitation of the water supply. Figure 1.30 shows neutron images of the pods. From the water distribution in the pod, the formation of the pod parenchyma as well as the vascular system could be clearly observed. The formation of the wall in the pod was distinguished at an early stage, and the seeds seemed to emerge from the pod parenchyma. The vascular system was shown to be connected to the shrunken

wall. This rape seed pod imaging is an example, but pod visualization is applicable to various developments in agricultural technology, especially the formation of sterile plants, where nondestructive analysis is needed.

1.3 Summary and Further Discussion

The neutron images provide water-specific images of plants that are not obtainable with other means. The CCD camera employed had the highest resolution (approximately 16 μm) of any other CCD camera available. One pixel in the figure corresponded to approximately 16 μm; therefore, we considered the resolution of the image to be approximately 16 μm. We expect that a CCD camera with higher resolution will be developed and that the water movement inside single cells might be able to be analyzed by neutron imaging.

The neutron imaging of roots was introduced. Through neutron imaging, morphological development of the roots imbedded in soil and water movement close to the root could be visualized, and not only 2D images but also the construction of 3D images enabled analysis of the morphological pattern of the roots and the water profile in soil.

Image analysis of the roots imbedded in soil showed that the water absorption activity in the roots gradually shifted downward from the upper to the lower part. Additionally, from the images adjacent to the root, the water absorption activity at the specific site of the root increased before development of the side roots. The water amount near the root had a gradient that increased drastically from 1 mm from the root surface toward the root, but the root surface was still not saturated with water. The space around the root surface was clearly observed when a 3D image of the root was created. In particular, the dissection image of the root imbedded in soil showed a water-deficient area in the vicinity of the main root surface, from the upper to the lower part. This suggests that there is hardly any contact between water solution and the root surface, which might indicate that the roots are absorbing water vapor rather than water solution. The root tip is always searching for a favorable location and creating space for the root tip to grow in the soil by circumnutation. In the case of a rice plant, one cycle of root tip rotation was found to take 50 min (see Chap. 8). Therefore, there is always a space in the vicinity of the root surface. If the roots absorb water vapor, the absorption of nutritional elements, including metals, from the roots should be drastically different from that of roots growing in water culture. Are the roots absorbing metal vapor, too?

The orientation of root development is another interesting topic, but it was not discussed much here. How does the root decide the direction of the growth? When VA mycorrhizal fungus was placed in a thin box and neutron images were taken, one of the side roots of a soybean plant developed linearly toward the fungus, which was more than 5 cm from the root (data not shown). Whether the hyphae induced the root pattern or not was not discernible.

The analysis of the morphological development of the root enabled us to evaluate the condition of the soil, especially in the development of soil fertilizer, soil conditioners or supplying devices of water. However, there was no reproducibility in the formation of the root pattern, since it is impossible to prepare exactly the same soil conditions for root growth. Therefore, as one solution to evaluate the soil condition based on root development, we measured the root length after formation of the line profile of the root as an indicator to compare growing conditions.

In the case of flower imaging, the water profile within the stem, bulb or pod could be visualized. Water movement derived from neutron imaging suggests tissue-specific functions for water, such as in stems. The bending neck phenomenon suggested another function of the stem. In the case of a rose plant, all of the stem close to the flower consisted of living cells, whereas in other plants, pith was formed where dead cells were packed. During a water-deficient period, living cell activity might cease and thereby prevent water movement toward flower parts. When the pith consisted of dead cells, it could be assumed that water might move easily by capillary phenomena. It was interesting to note that the function of dead cells might also be taken into account.

Many approaches are attempted to extend flowering; one of them is to change the viscosity of water, such as by dissolving an inert gas, such as Xe gas. When water containing dissolved Xe gas was supplied to a carnation flower, the flower took longer to become senescent, suggesting that the water loss due to transpiration was decreased. How water movement is controlled was proposed to provide clues regarding plant activities.

The visualization of green moisture in a wood disk was the first example. There were some other applications of neutron imaging in wood samples, such as detection of wood discoloration in a canker fungus-inoculated Sugi [2] or to measure the decay resistance of chemically modified wood [14], etc. The visualization of drying process of Sugi was presented in this chapter. Because Sugi is a popular type of lumber in Japan for building houses or furniture, and only one species exists. Even among the same cultivar of Sugi, the water content in the heartwood drastically varies. It is not known what causes the differences in moisture content in the heartwood. Water distribution within the wood disk showed a water gradient pattern within each annual ring so that the number of the water peaks was the same as the number of annual rings. In the case of Sugi, there was a difference in water content between heartwood and sapwood, and there were always a few water-deficient annual rings at the boundary between heartwood and sapwood, called white rings. However, the size of the white ring increases as the heartwood and sapwood grow. Then, how is water moved across this white ring toward the heartwood while maintaining the white ring? With the development of the tree, the size of the heartwood increases, and white rings are still formed between the heart and sapwood. That is, the white ring grows and maintains a low amount of water, whereas the amount of water in the heartwood or sapwood is maintained during growth. Is there any system to increase the size of this white ring containing a low amount of water?

There are many possibilities for the application of neutron imaging techniques to study plant samples. The neutron images acquired revealed new aspects of plant activity but raised many questions at the same time. Some of the questions raised were about root activities, but another interesting question was about the function or role of dead cells. The dead cells support the plant activities of living cells, which could be estimated through water images; however, how the dead cells are used efficiently is not known. Another question is how plants control water movement. The movement of water is a kind of engine that induces not only water absorption but also growth. It seemed that water movement was not derived simply from diffusion or osmotic pressure.

Though neutron imaging showed static water images of the plant samples, when successive static images were taken, it was possible to estimate the plant activity based on water movement, since the movement of the plants is rather slow.

Then, in the next section, the real movement of water in a living plant is presented utilizing radioisotopes.

Bibliography

1. Nakanishi TM, Matsubayashi M (1997) Nondestructive water imaging by neutron beam analysis in living plants. J Plant Physiol 151:442–445
2. Nakanishi TM, Okuni Y, Furukawa J, Tanoi K, Yokota H, Ikeue N, Matsubayashi M, Uchida H, Tsuji A (2003) Water movement in a plant sample by neutron beam analysis as well as positron emission tracer imaging system. J Radioanal Nucl Chem 255(1):149–153
3. Saito K, Nakanishi TM, Matsubayashi M, Meshitsuka G (1997) Development of new lignin derivatives as soil conditioning agents by radical sulfonation and alkaline-oxygen treatment. Mokuzai Gakkaishi 43(8):669–677. (Japanese)
4. Nakanishi TM, Matsumoto S, Kobayashi H (1993) Water hydrology by neutron radiography when water absorbing polymer was added to the soil. Radioisotopes 42:30–34
5. Okuni Y, Furukawa J, Matsubayashi M, Nakanishi TM (2001) Water accumulation in the vicinity of a soybean root imbedded in soil revealed by neutron beam. Anal Sci 17 (supplement):1499–1501
6. Furukawa J, Nakanishi TM, Matsubayashi M (2001) Water uptake activity in soybean root revealed by neutron beam imaging. Nondestr Test Evaluat 16:335–343
7. Nakanishi TM (2009) Neutron imaging applied to plant physiology. In: Anderson IS, McGreevy RL, Bilheux HZ (eds) Neutron imaging and applications, a reference for the imaging community. Springer, Cham, pp 305–317
8. Habu N, Nagasawa Y, Samejima M, Nakanishi TM (2006) The effect of substituent distribution on the decay resistance of chemically modified wood. Int Biodeterior Biodegradation 57:57–62
9. Nakanishi TM, Furukawa J, Matsubayashi M (1999) A preliminary study of CT imaging of water in carnation flower. Nucl Instrum Methods Phys Res A424:136–141
10. Matsushima U, Ooshita T, Nakanishi TM, Matsubayashi M, Seo Y, Kawagoe Y (2000) Effect of non-polar- gas on water in cut carnation flowers. Journal of the Japanese Society of Agricultural. Machinery 62(5):70–78
11. Nakanishi TM, Okano T, Karakama I, Ishihara T, Matsubayashi M (1998) Three dimensional imaging of moisture in wood disk by neutron beam during drying process. Holzforschung 52:673–676
12. Nakanishi TM, Matsubayashi M (1997) Water imaging of seeds by neutron beam. Bioimages 5 (2):45–48

13. Nakanishi TM, Inanaga S, Kobayashi H (1991) Non-destructive analysis of rape plant pod by neutron radiography. Radioisotopes 40:126–128
14. Yamada T, Oki Y, Yamato M, Komatsu M, Kusumoto D, Suzuki K, Nakanishi TM (2005) Detection of wood discoloration in a canker fungus-inoculated Japanese cedar by neutron radiography. J Radioanal Nucl Chem 264:329–332